Observing the Onset of Effective Mass

Rockson Chang,[1,*] Shreyas Potnis,[1] Ramon Ramos,[1] Chao Zhuang,[1] Matin Hallaji,[1] Alex Hayat,[1,2] Federico Duque-Gomez,[1] J. E. Sipe,[1] and Aephraim M. Steinberg[1]

[1]*Department of Physics and Institute of Optics, University of Toronto, 60 St. George Street, Toronto, Ontario M5S 1A7, Canada*

[2]*Department of Electrical Engineering, Technion, Haifa 32000, Israel*

(Received 5 March 2013; revised manuscript received 14 October 2013; published 2 May 2014)

The response of a particle in a periodic potential to an applied force is commonly described by an effective mass, which accounts for the detailed interaction between the particle and the surrounding potential. Using a Bose-Einstein condensate of ^{87}Rb atoms initially in the ground band of an optical lattice, we experimentally show that the initial response of a particle to an applied force is in fact characterized by the bare mass. Subsequently, the particle response undergoes rapid oscillations and only over time scales that are long compared to those of the interband dynamics is the effective mass observed to be an appropriate description. Our results elucidate the role of the effective mass on short time scales, which is relevant for example in the interaction of few-cycle laser pulses with dielectric and semiconductor materials.

DOI: 10.1103/PhysRevLett.112.170404 PACS numbers: 05.60.Gg, 37.10.Jk, 67.85.-d, 72.20.-i

The concept of the effective mass is ubiquitous in solid state physics, allowing for a simple semiclassical treatment of the response of a particle in a solid to an external force. The interaction with the surrounding potential dresses the particle with an effective mass, distinctly different from its bare mass, and allows for a description of the particle's dynamics based on Newton's second law [1]:

$$\langle a \rangle = \frac{F}{m_N^*(k)}, \tag{1}$$

where $\langle a \rangle$ is the average acceleration of the particle under an applied force F, and $m_N^*(k)$ is the effective mass for a particle with momentum k and band index N. The effective mass is inversely related to the curvature of the dispersion relation, and in one dimension is given by

$$m_N^*(k) = \hbar^2 \left[\frac{d^2}{dk^2} E_N(k) \right]^{-1}, \tag{2}$$

where $E_N(k)$ is the energy of the state, and $\hbar$ is Planck's constant. The modern description of electronic conduction in solids is intimately tied to the concept of the effective mass.

However, a direct application of Ehrenfest's theorem [2] shows that, for a particle in one band, the acceleration due to an applied force is F/m_0, where m_0 is the bare mass, and not F/m^*. In fact, a response characterized by m^* requires contributions from Bloch states in neighbouring bands, although these amplitudes may be small [3,4]. The multiband states that result in the effective mass behavior are naturally achieved when the force is applied slowly compared to the time associated with the band-gap frequency [5,6]. In contrast, when the force is abruptly applied the wave function initially remains unchanged, yielding a response described by m_0. Over time, the external force inevitably couples the initial and neighbouring bands, resulting in an acceleration which itself oscillates around F/m^* (see Fig. 1). In the presence of interband dephasing these oscillations die out. The steady state however contains small contributions from neighbouring bands, as

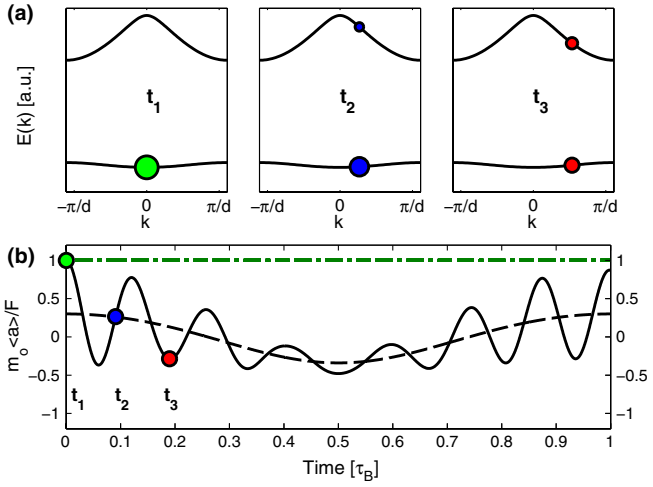

FIG. 1 (color online). Illustration of effective mass dynamics. (a) Lattice dispersion relation showing the time evolution of an initially single-band wave packet under an abruptly applied force F. (b) The corresponding acceleration $\langle a \rangle$. Over time scales that are long compared to one over the band-gap frequency, the acceleration is characterized by the lattice effective mass m^* and leads to Bloch oscillations (dashed black line). However the initial response of the single-band state is characterized by the bare mass m_0 (bare mass response shown by green dash-dotted line), and then rapidly oscillates around the usual effective mass behaviour.

imposed by the force, such that the total acceleration tends to F/m^* [7]. We use the term "dynamical mass" to refer to the mass associated with this transient response of the particle, and "effective mass dynamics" to refer to its variation in time. See Supplemental Material [8] for further details on the theoretical description.

In typical solid state systems, the fast time scales of the transient oscillations and dephasing effects have thus far prohibited observation of the effective mass dynamics. However, recent advances in attosecond science now allow for the generation of few-cycle, near-infrared laser pulses [9,10]. The study of the effects of these pulses on solid targets has garnered significant interest for ultrafast current control [11,12] and high-harmonic generation [13–15]. As the drive frequency approaches the band-gap frequency, the usual approximation of lattice effective mass response for conduction electrons is expected to become invalid, and it has been suggested that this breakdown will lead to decreased efficiency for high-harmonic generation in the subcycle regime [16]. Ultracold atoms in optical lattices have recently been suggested as a system in which the deviation from effective mass behavior is readily accessible [4]. The inherent length and time scales of ultracold atoms make them an ideal system to observe long-range, quantum coherent phenomena that occur in condensed matter physics but may be difficult to observe in the solid state [5,17–24].

In this Letter we report on the first observation of the effective mass dynamics of ultracold atoms in an optical lattice. By abruptly applying an external force, we show that the particle's initial response is characterized by the bare mass and is indifferent to the presence of the lattice. Subsequently, the response exhibits rapid oscillations at the band-gap frequency, and slow Bloch oscillations which are characterized by the usual effective mass.

We perform our experiment with a Bose-Einstein condensate of ^{87}Rb prepared in a hybrid optical and magnetic trap [25]. This trap is formed by the overlap of a single-beam optical dipole trap with a quadruople magnetic trap. The resulting potential has cylindrical symmetry with radial and axial harmonic trapping frequencies $f_r = 80$ Hz and $f_z = 20$ Hz, respectively. In this trap we produce nearly pure condensates of about 10^5 atoms. We then ramp up a laser standing-wave pattern over 100 ms, adiabatically loading our atoms into the ground state of a one-dimensional optical lattice with lattice constant $d = \lambda/2 = 532$ nm. The total potential has the form

$$U = U_L \cos^2(k_r z) - F(t) z, \tag{3}$$

where U_L is the lattice depth, and $F(t)$ the applied force (initially zero). The photon wave vector $k_r = 2\pi/\lambda$ sets characteristic momentum and energy scales, $\hbar k_r$ and $E_r = \hbar^2 k_r^2/2m_0$, respectively. We express the lattice depth in terms of the recoil energy via the dimensionless parameter $s = U_L/E_r$. The lattice potential generated in this way is essentially defect-free, and thus avoids the complications due to scattering that arise in typical solid state systems. The peak atomic density in the lattice is less than 3×10^{13} atoms/cm^3. In this regime interparticle interactions have been shown to be negligible up to a minor correction to the lattice depth [17]. We estimate the lattice depth based on the first-order diffraction amplitude for the $k = 0$ Bloch state. Comparing to a simulation of the Gross-Pitaevskii equation (GPE), we find that the dynamics occur as if the lattice had a depth $U_{\text{eff}} < U_L$. Our results are thus compared to a single-particle analysis at lattice depth U_{eff}, which for our typical densities, represents a correction of less than 10%. For our typical lattice depths and forces we can neglect interband Landau-Zener tunneling [26].

To initiate the effective mass dynamics, we abruptly shift the center of the magnetic trap, exerting a force F on our atoms along z that is essentially spatially uniform over the extent of our 20 μm sample. This shift is performed in 20 μs, and is much faster than the typical time scale corresponding to the band gaps in our experiment (around 100 μs). The effective mass dynamics result in oscillations of the average acceleration $\langle a \rangle$, and thus the average velocity $\langle v \rangle$. After a variable evolution time in the lattice we abruptly switch off all trapping potentials. The abrupt turn-off of the lattice preserves the momentum distribution, which we measure by imaging after time-of-flight (TOF) expansion.

Figure 2 shows the results of a typical experimental run. The free-space momentum distribution [Figs. 2(a) and 2(b)] is a diffraction pattern consisting of components separated by the recoil momentum $2\hbar k_r$ (the recoil velocity is $v_r = \hbar k_r/m_0 = 4.3$ μm/ms). The amplitude and velocity of each peak are extracted from a fit of four equally spaced, equal-width Gaussians [Figs. 2(c) and 2(d)]. The average velocity of the particles in the lattice as a function of time is then reconstructed from a weighted sum of these peaks [Fig. 2(e)]. We observe a clear oscillation in the average velocity on a millisecond time scale, consistent with Bloch oscillations [5,6,17,27]. This phenomenon arises due to the long-range, interwell coherence of the condensate and occurs at a frequency $\omega_B = Fd/\hbar$ [28,29]. In addition to the Bloch oscillation we observe much faster oscillations on a 100 μs time scale, consistent with dynamics at the band-gap frequency. This is observed to arise due to a modulation of the relative amplitudes of the diffracted momentum components. In the tight-binding limit, these dynamics may be thought of in terms of the intrawell wave packet oscillations which occur at the band-gap frequency in parallel with the slower, long-range Bloch oscillations (see Supplemental Material [8]). The corresponding GPE simulation is shown in Figs. 2(f)–2(h) for $s = 10$ and $F/m_0 = 12.3$ μm/ms^2. These parameters were chosen to match the frequency of the fast and slow oscillations of

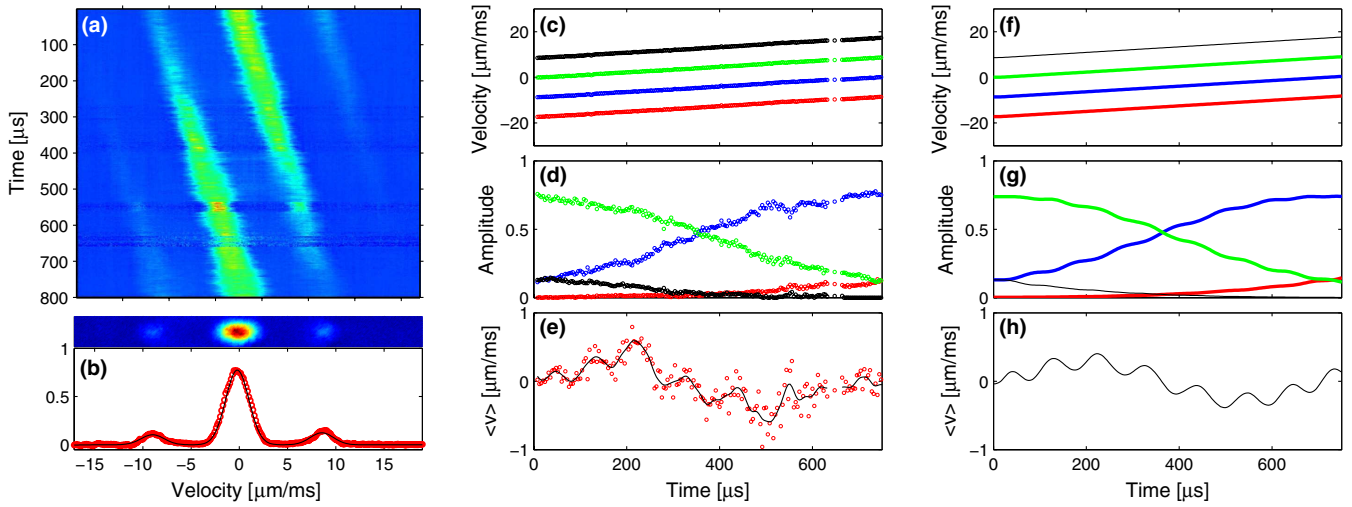

FIG. 2 (color online). Observation of effective mass dynamics. $s = 9.4$ and $F/m_0 = 11.7$ μm/ms^2. (a) Composite of absorption images. Each row is a slice of an image taken after variable evolution time in the lattice (4 μs resolution) and 20 ms TOF. Color scale: from blue to red, indicates increasing optical density. (b) Example absorption image, and one-dimensional profile and fit. (c)–(e) The velocity and amplitude of each peak, and the reconstructed average velocity of the distribution. The gap in the data at 650 μs due to poor condensate preparation during these runs. The solid black curve is the result of low-pass filtering this data, serving as a guide to the eye. (f)–(h) Corresponding GPE simulation (see text).

the data, respectively, and are in agreement with the measured parameters within experimental uncertainty.

Under the abruptly applied force, the initially single-band state will acquire amplitudes in adjacent bands over time. The coupling to these additional bands provides contributions to the average acceleration that will oscillate at the respective energy differences. For narrow momentum width wave packets and times shortly after the force is applied, the acceleration is given by [3,4]

$$\langle a(t)\rangle = \frac{F}{m_0}\left[\frac{m_0}{m_N^*} + \sum_{n\neq N}\frac{2}{m_0}\frac{p_{nN}^2}{\Delta_{nN}}\cos(\Delta_{nN}t/\hbar)\right], \quad (4)$$

where $\Delta_{nN} = E_n - E_N$ and p_{nN} are the energy gap and momentum matrix element between Bloch states in bands n and N, respectively. At $t = 0$ the contributions to $\langle a\rangle$ are in phase and the initial acceleration is that of a particle with bare mass, as expected from Ehrenfest's theorem, and can be seen in Eq. (4) by applying the effective mass sum rule [3]. For a particle initially in the ground band ($N = 1$), the coupling is primarily to the first excited band ($n = 2$), and the effective mass dynamics in this two-band case are governed entirely by the band gap Δ_{21}. As the particle traverses the Brillouin zone during a Bloch cycle, the band gap changes, resulting in a variation in the amplitude and frequency of the effective mass oscillation. These complex oscillations are the effective mass dynamics.

To study the dynamics, we fit the average velocity to the sum of two sinusoids, explicitly separating the Bloch oscillation from the effective mass dynamics,

$$v(t) = A_d\sin(\omega_d t - \phi_d) + A_B\sin(\omega_B t - \phi_B), \quad (5)$$

where A is the amplitude, ω the frequency, and ϕ the phase of the oscillations. The subscripts d and B indicate parameters for the effective mass oscillation and Bloch oscillation, respectively. Due to the variation of the band gap across the Brillouin zone, this fitting function is not strictly correct at times comparable to the Bloch period. Equation (5) is a compromise between capturing as many of the features of the dynamics as possible while still obtaining reliable fits. When extracting the effective mass oscillation we fit only the first 300 μs of data (roughly three periods of the fast oscillation) to obtain an accurate estimate of the effective mass dynamics near the center of the band ($k = 0$).

Figure 3 plots the dependence of these time scales on the applied force F and lattice depth s. The frequency of the slow oscillation, f_B, is observed to scale linearly with the applied force [Fig. 3(a), lower], as expected for Bloch oscillations. We also plot this frequency, scaled by the applied force, against lattice depth [Fig. 3(b), upper] to show that the frequency is independent of lattice depth. The fast oscillation frequency, f_d, increases with lattice depth [Fig. 3(b), lower] and thus the band gap, but is independent of applied force [Fig. 3(a) upper]. The fitted frequency is compared to the calculated band gap at $k = 0$ and $k = k_r$, representing the range of frequencies the particle samples as it undergoes a complete Bloch oscillation. A more direct comparison to the data is made by fitting Eq. (5) to the first 300 μs of data generated from a GPE simulation, in the same way as we fit to the experimental data.

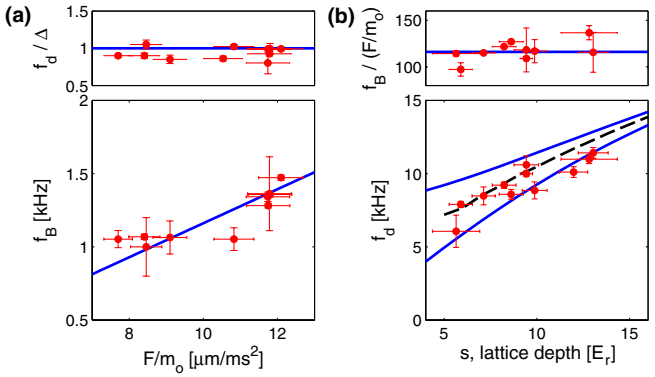

FIG. 3 (color online). (a) Variation of dynamical mass frequency (upper) and Bloch frequency (lower) with applied force. The dynamical mass frequency, normalized by Δ, is expected to be independent of the force. The Bloch frequency scales linearly with the applied force. (b) Variation in Bloch frequency (upper) and dynamical mass frequency (lower) with lattice depth. The Bloch frequency, normalized by F/m_0, is expected to be a constant $m_0 d/h$ (blue solid line). The dynamical mass frequency is compared to the band gap at $k = 0$ and $k = k_r$ (upper and lower solid blue lines, respectively), and to simulated data fitted to Eq. (5) (dashed black curve).

From the average velocity fits we extract the initial response to the applied force (Fig. 4). The external force is applied within 20 μs after a 20 μs delay. This delay is accounted for by the phase in the sinusoids of our fitting function. The initial response is evaluated at time $t_0 = \phi_d/\omega_d$, when the phase of the fast oscillation is zero. The effective mass theorem Eq. (1) describes the response

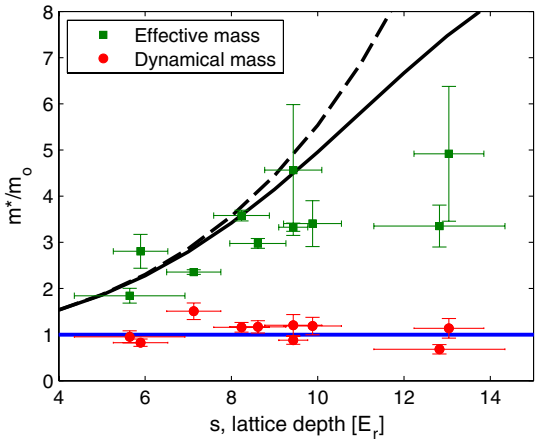

FIG. 4 (color online). Effective mass and dynamical mass results. The effective mass at the center of the ground band associated with the Bloch oscillation is plotted as green squares. As the lattice depth increases, the effective mass is expected to increase (dashed black line). Accounting for the finite imaging window skews the expected m^* down (solid black line; see text). The initial ($t = 0$) dynamical mass is extracted from the full dynamics (red circles), and is expected to be consistent with the bare mass response $m^*/m_0 = 1$, independent of lattice depth (solid blue line).

of a particle to a force over time scales that are long compared to the interband dynamics; thus, we estimate this effective mass from the Bloch oscillation alone. Since the band curvature decreases with increasing lattice depth, the effective mass increases. However, the full response contains contributions from both the slow Bloch oscillations and the fast effective mass dynamics. The dynamical mass is estimated from the sum of these contributions, and at t_0 is observed to be consistent with the bare mass, independent of lattice depth.

In deep lattices ($s > 10$), the deduced effective mass begins to deviate from the predictions. This is partially due to the growth of high-order diffraction peaks in the momentum distribution which lie beyond our imaging window. Neglecting these peaks causes us to overestimate the amplitude of the Bloch oscillation, and thus underestimate the effective mass. Despite this correction, we find that our measured amplitude for Bloch oscillation is larger than expected (see sample data and simulation in Fig. 2), leading to an estimated effective mass smaller than expected. This effect is only prominent in the deep lattice regime, whereas the bulk of our data are for lattice depths of $s < 10$. The deviation in A_B may be a band-mapping effect due to the finite turn-off time of the optical lattice [23,24], which is expected to be more prominent in the deep lattice regime. Note that this has a minimal impact on the estimate of the dynamical mass since the dominant contribution in the deep lattice regime is from the effective mass dynamics. The error bars are given by the fit uncertainties, where the main contribution in the effective mass uncertainty comes from fitting the long time scale Bloch oscillation. In the presence of excited band decay and interband dephasing, the effective mass dynamics are expected to reduce to the behavior described by the usual effective mass. In our system, this can occur due to interparticle scattering [30,31]. Within the parameter range probed, we do not expect to see dephasing of the effective mass oscillation.

To our knowledge, the effective mass dynamics explored in this work have never before been observed, despite their initial prediction nearly 60 years ago. Whereas past work on Bloch oscillations focused on time scales that are long compared to that of the interband dynamics, our work clarifies the role of the effective mass on short time scales, requiring comparatively fast excitation and fine temporal resolution. These results shed experimental light on one of the most fundamental aspects of motion in a lattice, and should be directly relevant to a broad range of experiments on ultrafast dynamics in a variety of systems, for example in the control of electron dynamics in a solid on a subfemtosecond time scale [4,10–14].

The authors thank A. Jofre, M. Siercke, and C. Ellenor for their work in developing the Bose-Einstein condensation apparatus, A. Stummer for providing technical support, and M. Ivanov and O. Smirnova for fruitful discussions. We acknowledge support from NSERC and CIFAR.

*Present address: Laboratoire Charles Fabry, Institut d'Optique, CNRS, Univ Paris-Sud, 2 Avenue Augustin Fresnel, 91127, Palaiseau Cedex, France.
rockson.chang@u-psud.fr

[1] N. W. Ashcroft and N. D. Mermin, *Solid State Physics* (Saunders College, Rochester, NY, 1976).
[2] D. Pfirsch and E. Spenke, Z. Phys. **137**, 309 (1954).
[3] K. Hess and G. Iafrate, Proc. IEEE **76**, 519 (1988).
[4] F. Duque-Gomez and J. E. Sipe, Phys. Rev. A **85**, 053412 (2012).
[5] M. Ben Dahan, E. Peik, J. Reichel, Y. Castin, and C. Salomon, Phys. Rev. Lett. **76**, 4508 (1996).
[6] T. Pertsch, P. Dannberg, W. Elflein, A. Bräuer, and F. Lederer, Phys. Rev. Lett. **83**, 4752 (1999).
[7] E. N. Adams and P. N. Argyres, Phys. Rev. **102**, 605 (1956).
[8] See Supplemental Material at http://link.aps.org/supplemental/10.1103/PhysRevLett.112.170404 for a more detailed theoretical description of the effective mass dynamics.
[9] T. Brabec and F. Krausz, Rev. Mod. Phys. **72**, 545 (2000).
[10] F. Krausz and M. I. Stockman, Nat. Photonics **8**, 205 (2014).
[11] A. Schiffrin, T. Paasch-Colberg, N. Karpowicz, V. Apalkov, D. Gerster, S. Mühlbrandt, M. Korbman, J. Reichert, M. Schultze, S. Holzner, J. V. Barth, R. Kienberger, R. Ernstorfer, V. S. Yakovlev, M. I. Stockman, and F. Krausz, Nature (London) **493**, 70 (2013).
[12] M. Schultze, E. M. Bothschafter, A. Sommer, S. Holzner, W. Schweinberger, M. Fiess, M. Hofstetter, R. Kienberger, V. Apalkov, V. S. Yakovlev, M. I. Stockman, and F. Krausz, Nature (London) **493**, 75 (2013).
[13] S. Ghimire, A. D. DiChiara, E. Sistrunk, P. Agostini, L. F. DiMauro, and D. A. Reis, Nat. Phys. **7**, 138 (2011).
[14] S. Ghimire, A. D. DiChiara, E. Sistrunk, G. Ndabashimiye, U. B. Szafruga, A. Mohammad, P. Agostini, L. F. DiMauro, and D. A. Reis, Phys. Rev. A **85**, 043836 (2012).
[15] M. Ivanov and O. Smirnova, Chem. Phys. **414**, 3 (2013).
[16] P. Hawkins, M. Ivanov, and V. Yakovlev (private communication).
[17] O. Morsch, J. H. Müller, M. Cristiani, D. Ciampini, and E. Arimondo, Phys. Rev. Lett. **87**, 140402 (2001).
[18] S. R. Wilkinson, C. F. Bharucha, K. W. Madison, Q. Niu, and M. G. Raizen, Phys. Rev. Lett. **76**, 4512 (1996).
[19] J. Billy, V. Josse, Z. Zuo, A. Bernard, B. Hambrecht, P. Lugan, D. Clément, L. Sanchez-Palencia, P. Bouyer, and A. Aspect, Nature (London) **453**, 891 (2008).
[20] G. Roati, C. D'Errico, L. Fallani, M. Fattori, C. Fort, M. Zaccanti, G. Modugno, M. Modugno, and M. Inguscio, Nature (London) **453**, 895 (2008).
[21] J.-P. Brantut, J. Meineke, D. Stadler, S. Krinner, and T. Esslinger, Science **337**, 1069 (2012).
[22] D. Stadler, S. Krinner, J. Meineke, J.-P. Brantut, and T. Esslinger, Nature (London) **491**, 736 (2012).
[23] J. H. Denschlag, J. E. Simsarian, H. Häffner, C. McKenzie, A. Browaeys, D. Cho, K. Helmerson, S. L. Rolston, and W. D. Phillips, J. Phys. B **35**, 3095 (2002).
[24] A. Browaeys, H. Häffner, C. McKenzie, S. L. Rolston, K. Helmerson, and W. D. Phillips, Phys. Rev. A **72**, 053605 (2005).
[25] Y.-J. Lin, A. R. Perry, R. L. Compton, I. B. Spielman, and J. V. Porto, Phys. Rev. A **79**, 063631 (2009).
[26] C. F. Bharucha, K. W. Madison, P. R. Morrow, S. R. Wilkinson, B. Sundaram, and M. G. Raizen, Phys. Rev. A **55**, R857 (1997).
[27] K. Leo, P. H. Bolivar, F. Brggemann, R. Schwedler, and K. Khler, Solid State Commun. **84**, 943 (1992).
[28] F. Bloch, Z. Phys. **52**, 555 (1929).
[29] C. Zener, Proc. R. Soc. A **145**, 523 (1934).
[30] R. Morandotti, U. Peschel, J. S. Aitchison, H. S. Eisenberg, and Y. Silberberg, Phys. Rev. Lett. **83**, 4756 (1999).
[31] M. Gustavsson, E. Haller, M. J. Mark, J. G. Danzl, G. Rojas-Kopeinig, and H.-C. Nägerl, Phys. Rev. Lett. **100**, 080404 (2008).